ACS Photonics

Article

pubs.acs.org/journal/apchd5

Interatomic Coupling of Au Molecular Clusters and Er^{3+} Ions in Silica

Tiziana Cesca,*[,†] Boris Kalinic,[†] Chiara Maurizio,[†] Carlo Scian,[†] Giancarlo Battaglin,[‡] Paolo Mazzoldi,[†] and Giovanni Mattei[†]

[†]Physics and Astronomy Department and CNISM, University of Padova, via Marzolo 8, I-35131 Padova, Italy

[‡]Department of Molecular Sciences and Nanosystems, Ca' Foscari University of Venice, Dorsoduro 2137, I-30123 Venice, Italy

Supporting Information

ABSTRACT: To unveil the mechanisms of energy transfer between Au_N nanostructures and Er^{3+} ions in silica is of paramount importance for the possible use of Au molecular clusters as sensitizing agents of the rare-earth luminescence in photonic devices. In the present work a phenomenological model was developed that allowed us to estimate the most important photophysical parameters as the sensitization cross-section, the fraction of sensitized Er ions, and the coupling distance of the energy transfer. The results demonstrate that in spite of very large sensitization cross-sections (more than 3 orders of magnitude higher than the intrinsic Er excitation cross-section in silica) only a limited fraction of Er ions (<1%) are indirectly excited by the Au_N nanoclusters, and the energy transfer occurs via short-range coupling at interatomic distances, in the range 0.4−0.8 nm.

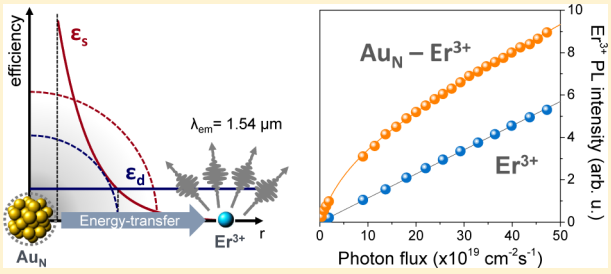

KEYWORDS: *gold molecular clusters, erbium, energy transfer, short-range coupling, photoluminescence enhancement, ion implantation*

The luminescence properties of rare-earth elements have been the object of intense interest of the scientific community for decades.[1,2] Among the trivalent lanthanides, Er^{3+} in particular gained major importance for its radiative emission at 1.54 μm, and Er-doped silica-based materials became extremely interesting for photonic, optoelectronics, and quantum information applications.[3−11] The incorporation of the rare earth in an inorganic matrix has the advantage of significantly improving its thermal and photochemical stability. Nonetheless, strong limitations to the realization of efficient photonic devices are related to the small cross-section for Er excitation, which is typically of the order of 10^{-21}−10^{-19} cm^2, depending on the matrix.[6] The interaction with sensitizing species to enhance the Er pumping efficiency represents a possible solution to this problem, and different approaches have been explored in these years using other rare-earths,[12,13] silicon nanocrystals,[14−19] or metallic nanostructures.[20−25] Concerning metallic nanoclusters (NCs), the Er^{3+} luminescence sensitization by Au NCs has been revealed by our group in Er−Au coimplanted silica systems.[25] Such study combined photoluminescence measurements to investigate the Er emission properties and X-ray absorption spectroscopy characterizations to follow the Au cluster nucleation and growth at the very early stages. The results showed that subnanometric Au nanoclusters are very efficient sensitizers for the Er emission. The dominant pumping mechanism of the Er ions was demonstrated to be a nonresonant energy-transfer process mediated by the broadband interband absorption of the Au nanoclusters. Plasmonic field enhancement effects due to metallic nanoparticles as well as a possible role of implantation-induced defects on the Er sensitization have also been ruled out.[25−27]

The energy transfer is a complex process that is expected to depend on a variety of factors, involving the Au clusters (size distribution, numerical density, cluster structure), the Er site, and the matrix structure. In a very recent work, by studying the luminescence properties of molecule-like Au nanoclusters obtained by ion implantation in silica, we demonstrated that the process is triggered by the formation of a near-infrared Au-related luminescence band, resonant with a corresponding Er^{3+} absorption transition, that acts as a preferential de-excitation channel through which the energy is transferred from the Au NCs to the Er ions.[28] Furthermore, we demonstrated that the energy transfer occurs in a nonradiative way, and an upper limit to the interaction length of the process was given by the Au−Au intercluster semidistance.[29] In spite of these results, a precise estimation of the coupling distance as well as of the sensitization cross-section that characterize the energy-transfer process is very challenging to get and is still lacking. The knowledge of these parameters on the other hand is of paramount importance for the possible employment of molecular Au clusters as rare-earth sensitizers in specific photonic devices.

To this aim, in the present work we studied the Er-related luminescence properties of Er−Au codoped silica samples obtained by ion implantation at different fluences. To investigate in detail the interaction among Au sensitizers and Er ions the relative concentration of the two species in the samples was varied over more than 1 order of magnitude. This, coupled with proper annealing conditions, allowed a fine tuning

Received: August 6, 2014
Published: December 11, 2014

Table 1. Sample Preparation Conditions (Ion Implantation and Thermal Treatments)

samples series	ion	energy (keV)	current density (μA/cm^2)	fluence (ion/cm^2)	annealing temperature (°C)
Er1Au0.5	Er	50 + 100 + 190	0.05	6.7×10^{14}	800
	Au	60 + 110 + 190	0.05	3.4×10^{14}	300−800
Er1Au1	Er	50 + 100 + 190	0.05	6.7×10^{14}	800
	Au	60 + 110 + 190	0.05	6.7×10^{14}	300−800
Er0.7Au1	Er	50 + 100 + 190	0.05	4.7×10^{14}	800
	Au	60 + 110 + 190	0.05	6.7×10^{14}	300−800
Er0.4Au1	Er	50 + 100 + 190	0.05	2.7×10^{14}	800
	Au	60 + 110 + 190	0.05	6.7×10^{14}	300−800
Er1Au5	Er	50 + 100 + 190	0.05	6.7×10^{14}	800
	Au	60 + 110 + 190	0.1	3.4×10^{15}	300−800
Er0.7Au5	Er	50 + 100 + 190	0.05	4.7×10^{14}	800
	Au	60 + 110 + 190	0.1	3.4×10^{15}	300−800
Er1Au10	Er	50 + 100 + 190	0.05	6.7×10^{14}	800
	Au	60 + 110 + 190	0.1	6.7×10^{15}	300−800

of the Au cluster sizes in the subnanometer range. By systematic photoluminescence characterizations performed for both resonant and out-of-resonance Er excitation conditions we developed a phenomenological model through which the relevant photophysical aspects of the energy-transfer mechanism are unveiled. Then a quantitative estimation of the most important parameters, such as the sensitization cross-section, σ_{eff}, the fraction of sensitized Er ions, f_s, and the interaction distance, R_{int}, for the energy-transfer process was obtained.

METHODS

Samples Preparation. Triple energy Au implantations were performed on silica slides (Herasil I by Haereus) that were previously implanted with Er at a total fluence of 6.7×10^{14} cm^{-2} and annealed at 800 °C in N_2 atmosphere. For comparison, lower Er implantation fluences were also investigated (4.7×10^{14} cm^{-2} and 2.7×10^{14} cm^{-2}). The same implantation scheme was used for both Er and Au implantations producing almost constant concentration profiles of the two elements in an implanted region about 70 nm thick.[25] For this work, different sets of samples were produced in which the [Au]/[Er] concentration ratio was spanned over the range 0.5−10. The implantation fluences were measured by Rutherford backscattering spectrometry (RBS). After Au implantations isochronal annealings of the samples were performed for 1 h at different temperatures in the range 300−800 °C in inert (N_2) atmosphere to induce Au clustering and to recover the matrix from radiation damage. In the following the sample labels will indicate the Au concentration with respect to the Er one, the annealing temperature, and atmosphere: e.g., for the sample Er1Au5−N620 the Au concentration was about 5 times the Er one, and it was annealed at T = 620 °C in a nitrogen atmosphere. For all the sample series an Er-implanted silica sample (annealed at 800 °C in N_2 atmosphere), but without Au incorporation, was used as a reference for the photoluminescence measurements. For the series implanted with Er at a fluence of 6.7×10^{14} ions/cm^2 ([Er] = 1), this reference sample will be labeled as Er800. Details on the preparation conditions (ion implantation and thermal treatments) of the different samples' sets are reported in Table 1.

Optical Characterizations. Photoluminescence (PL) measurements were performed at room temperature using a cw Ar laser whose pumping lines at 488 and 476.5 nm allow for the Er^{3+} photostimulation in resonance (matching the $^4I_{15/2} \rightarrow {}^4F_{7/2}$ Er absorption transition) and out-of-resonance (i.e., the pumping radiation is not directly absorbed by the rare-earth), respectively. The laser lines were selected by interference filters. Broad-band excitation measurements were also obtained by pumping the samples with all the laser lines at the same time (i.e., without interference filters). The laser beam was mechanically chopped at 6 Hz. The luminescence signal was spectrally resolved by a single grating monochromator and detected by a N_2-cooled photomultiplier tube (Hamamatsu R5509-72). The spectra were recorded with a lock-in amplifier using the chopper frequency as a reference signal. PL measurements as a function of the photon flux were also performed. The photon flux was tuned by varying the pumping power and the area of the beam spot at the sample position. For all the measurement configurations the spot size was determined by the knife-edge method.[30] Time-resolved PL analyses were carried out by fixing the detected wavelength and collecting the PL intensity decay as a function of time with a transient digitizer (Tektronix TDS7104).

RESULTS AND DISCUSSION

The room-temperature PL emission intensity, measured at 1540 nm as a function of the annealing temperature, of Er−Au coimplanted silica samples thermally treated in a nitrogen atmosphere is reported in Figure 1. All the samples have an Er concentration of 9.6×10^{19} Er^+/cm^3, while different Au fluences were implanted in order to obtain a [Au]/[Er] concentration ratio that spans over more than 1 order of magnitude. The PL measurements have been performed upon resonant Er^{3+} excitation at 488 nm with a pump power of 22 mW. The horizontal dashed line indicates the PL signal level of the reference sample (Er800). In Figure S1 of the Supporting Information we have reported the PL spectra in the 1400−1700 wavelength range of the Er1Au1 samples annealed at the different temperatures. Analogous spectra have been measured for all the Er−Au coimplanted sample series investigated in the present work. The experimental data in Figure 1 have been measured by fixing the emission wavelength at 1540 nm and collecting the emitted PL intensity. Figure 1 shows that in the whole range of Au concentrations explored the temperature evolution of the PL intensity is characterized by an increase up to a maximum value and then the subsequent significant decrease down to PL signals similar to or lower than the value of the Er800 reference sample. In order to reproduce this trend we have fitted the experimental data with a Gaussian function

dx.doi.org/10.1021/ph500452q | ACS Photonics 2015, 2, 96−104

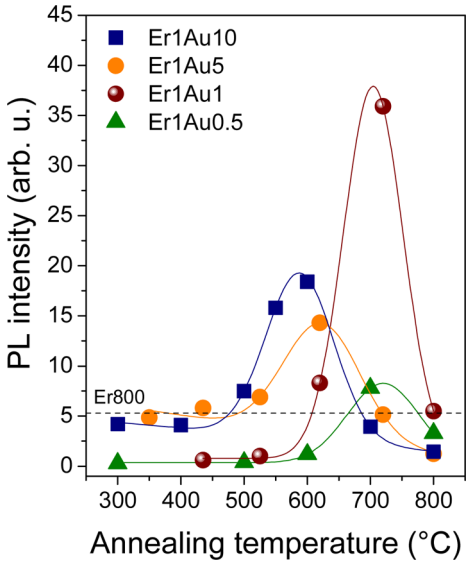

Figure 1. Room-temperature PL emission at 1540 nm as a function of the annealing temperature of Er−Au coimplanted samples thermally treated in an inert N_2 atmosphere. The samples are resonantly excited at 488 nm with a pump power of 22 mW. The solid lines are Gaussian fits as described in the text. The horizontal dashed lines indicate the PL intensity of the Er800 reference sample.

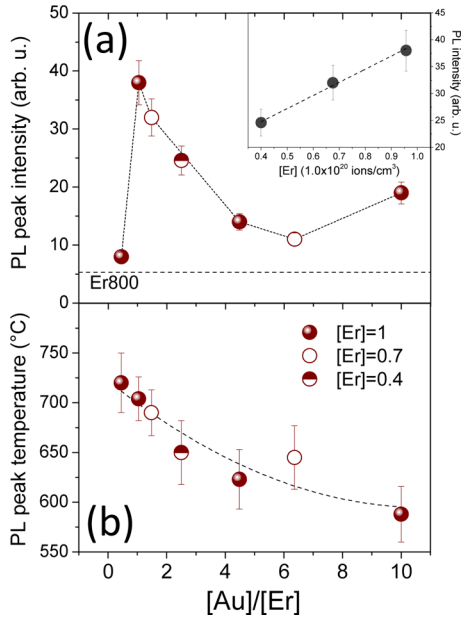

Figure 2. PL peak intensity (a) and PL peak temperature (b) as a function of the [Au]/[Er] concentration ratio of the different sample series. The red dots indicate the series of samples implanted with Er at a concentration of 9.6×10^{19} Er^+/cm^3 ([Er] = 1). The open circles are the data of the sample series Er0.7Au1 and Er0.7Au5, while the half-filled dot corresponds to the Er0.4Au1 series. The inset in panel (a) shows the trend of the PL intensity versus Er concentration at the constant Au concentration [Au] = 1 (i.e., about 1×10^{20} Au^+/cm^3).

(solid lines in Figure 1). For the samples with the highest Au concentrations (Er1Au5 and Er1Au10) a polynomial background has also been added to the Gaussian function to fit the low-temperature data. This background is needed to account for the PL signal that can be measured in these samples already at low annealing temperatures (T < 500 °C), which is instead negligible in the samples implanted at a lower Au fluence (Er1Au1 and Er1Au0.5 series). These fits have been used as a guide for the eye and to extract the peak parameters (PL peak temperature and peak intensity). The overall behavior exhibited by the samples shown in Figure 1 is consistent with the results of our previous work reported in ref 25. In that work the samples were analogous to the Er1Au10 samples studied here, but we see now that the reduction of the [Au]/[Er] ratio produces a decrease in the temperature at which the maximum PL emission occurs. Using the same framework to interpret the data, the first increase of the PL intensity is related to the progressive aggregation of dispersed Au atoms in small Au_N clusters as well as to the recovery of the matrix from radiation damage, while the observed decrease at higher temperatures is due to the further cluster growth that reduces the numerical density of ultrasmall clusters (i.e., with size smaller than 1 nm) demonstrated to be the most effective as sensitizers for Er emission.[25]

From the data in Figure 1 it emerges clearly that the Au implantation fluence has a remarkable effect on the temperature evolution of the PL emission, in particular on the peak position (peak temperature) and the maximum intensity. In order to highlight this effect we have plotted in Figure 2 the PL peak intensity (a) and the peak temperature (b) obtained from the Gaussian fits, as a function of the [Au]/[Er] concentration ratio. The open circles and the half-filled dot represent the results obtained from three different series of Er−Au coimplanted samples in which Er was implanted at a lower total fluence. Following the adopted notation these series can be indicated as Er0.7Au1, Er0.7Au5, and Er0.4Au1, respectively. The Au fluences are the same as for the Er1Au1 and Er1Au5 samples. These data can be treated consistently with those of all the other sample series, thus suggesting that the mechanisms to be considered are indeed dependent on the relative concentration of Au sensitizers and Er ions. As shown in Figure 2a, the evolution of the peak intensity as a function of the relative Au concentration with respect to Er is not monotonic but exhibits a maximum when the Au concentration equals the Er one ([Au]/[Er] = 1). On the contrary, the peak temperature (Figure 2b) is characterized by a monotonic decrease with increasing [Au]/[Er] ratio. The dashed line is a polynomial fit of the data. This behavior can be understood by taking into account that the Au implantation process followed by thermal treatments is expected to induce the growth of Au clusters with an average size which is smaller for lower Au fluences. The increase of the peak temperature for decreasing [Au]/[Er] concentration ratios is related to the growth of the Au NCs in the optimal size range for the Er sensitization (10−20 atoms)[25] that occurs at increasing annealing temperatures for decreasing Au concentrations. Moreover, by comparing the PL emission results measured from samples containing the same amount of gold but implanted with Er at different fluences (open circles and half-filled dot), it emerges that an increase of the maximum PL emitted intensity can be obtained when higher Er concentrations are incorporated in the samples. To highlight this effect we have reported in the inset of Figure 2a the PL intensity as a function of the Er concentration for the samples with the same Au concentration of about 1×10^{20} Au^+/cm^3 ([Au] = 1 in the adopted units). The graph shows a linear trend up to the Er concentration of 9.6×10^{19} Er^+/cm^3 ([Er] = 1). It is worth noting that this value corresponds to half of the reported limit for Er concentration quenching in silica.[31] For this reason, to rule out possible Er−Er cooperative effects which could mask or hinder the Au_N−Er interaction we limited

dx.doi.org/10.1021/ph500452q | ACS Photonics 2015, 2, 96−104

the maximum Er concentration investigated to this value and explored the effect of the Er concentration on the PL emission intensity by reducing it down to [Er] = 0.7 and [Er] = 0.4. In the hypothesis that the Au cluster configuration is the same and defining an interaction volume around the Au_N clusters for the Au_N–Er coupling, the observed linear trend of the PL emission versus Er concentration is consistent with the corresponding increase of the number of active Er ions in this volume. Nonetheless, it is important to point out that the data in Figure 2b show that the annealing temperature at which the maximum PL emission occurs varies as a function of the [Au]/[Er] concentration ratio, thus suggesting that the Er concentration has indeed an effect also on the Au cluster nucleation.

Further insights into the role of the Au_N clusters as Er sensitizers can be gained by studying the temporal decay of the Er^{3+} luminescent emission at 1540 nm. To this aim we performed time-resolved PL measurements of all the investigated samples. The PL temporal decays of the samples were characterized by a nonexponential trend and were fitted with a stretched exponential decay function leaving the lifetime (τ) and the stretching parameter (β) as free parameters for the calculations. As an example, Figure S2 of the Supporting Information shows the experimental PL temporal decay curves and the fitting results of the Er1Au1 samples annealed at different temperatures. The effective lifetime (τ_{eff}) of the Er^{3+} luminescent emission was then calculated through the function

$$\tau_{eff} = \frac{\tau}{\beta}\Gamma\left(\frac{1}{\beta}\right)$$

according to the method described in ref 25. $\Gamma(x)$ is the Eulerian gamma function.

In Figure 3 we have reported the results of these fittings obtained from the lifetime measurements of the samples under

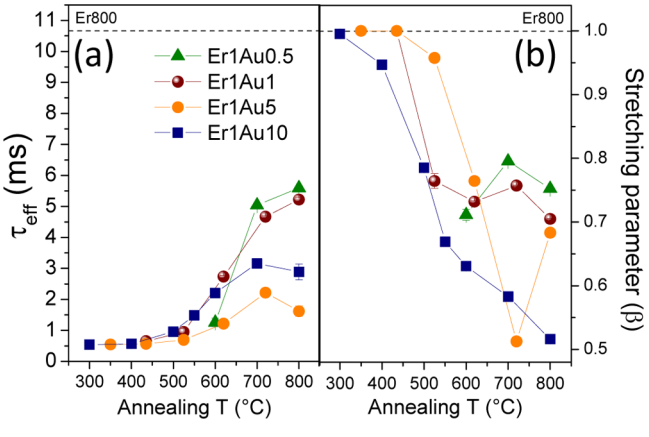

Figure 3. (a) Effective lifetime (τ_{eff}) and (b) stretching parameter (β) of the Er^{3+} PL emission at 1540 nm as a function of the annealing temperature of Er–Au coimplanted samples. The samples were resonantly excited at 488 nm.

resonant pumping conditions at 488 nm. Out-of-resonance (at 476.5 nm) lifetime measurements were also performed providing in all cases the same results. In both panels in Figure 3 the horizontal dashed line indicates the results of the Er800 reference sample. A single exponential decay ($\beta = 1$) was measured in this case with a lifetime $\tau^* = (10.7 \pm 0.1)$ ms. Considering the data reported in Figure 3(a) we can observe that for all the sample series the PL effective lifetime increases by increasing the annealing temperature. Moreover, at the highest annealing temperatures, the samples implanted at lower Au fluences are characterized by a τ_{eff} which is about twice the value determined from the samples implanted at higher Au fluences. This behavior is consistent with a progressive recovery upon annealing at increasing temperatures of irradiation defects that may act as nonradiative recombination centers, thus increasing the probability for the Er de-excitation, and the fact that a lower radiation damage level is induced by Au implantation at lower fluences.[26] Nonetheless, it is worth noting that even for the lowest Au fluence (Er1Au0.5 series) it is not possible to completely recover the emission lifetime of the Er800 reference sample. This shortening effect on the lifetime has to be ascribed to the presence of the Au nanoclusters in the samples acting as Er sensitizers and not to the formation of nonradiative recombination centers related to irradiation defects. Indeed in a recent paper we investigated the effects of implantation damage on the Er^{3+} luminescence properties in silica by studying Er–Xe coimplanted silica samples.[26] Xe was used in that case to induce in the samples implantation damage similar to Au. Even at the highest Xe implantation fluence (corresponding to the sample series Er1Au10 of this work) single exponential temporal decays of the PL emission were measured at all the annealing temperatures with lifetimes close to the values measured in the samples implanted with Er alone. The shortening effect on the lifetimes observed in the Er–Au coimplanted samples investigated in the present work thus indicates that the Au clusters play an active role in the Er emission that is not merely related to the activation of fast nonradiative de-excitation channels as a consequence of implantation: instead, the energy-transfer mechanisms have to be taken into account. It is worth noting that a further possible effect due to the modification of the local dielectric environment around the Er ions induced by the presence of the Au nanostructures cannot be definitely ruled out.[32] Nonetheless, due to the ultrasmall Au cluster size and the size distribution induced by the Au implantation process, a quantitative *a priori* estimation of such an effect is not possible, and its role can only be guessed.

Further information can be gained from the values of the stretching parameter (β) determined from the different samples (see Figure 3b). The stretching parameter indeed accounts for a dispersion in the relaxation rates of the Er ions caused by local inhomogeneities in the Er ion environment induced by the Au incorporation.[25] For all the Au fluences investigated in this work, the values of β are close to 1 (single exponential decay) for the samples annealed at low temperatures ($T < 500$ °C) and decrease for increasing annealing temperatures. This suggests that the Au cluster growth occurring at increasing annealing temperatures is accompanied by a corresponding increase of configurational disorder which is more pronounced when the Au fluence is higher. On the other hand, at the annealing temperatures that induce the maximum PL emission of the different sample series the stretching parameter is higher when the Au concentration is lower, indicating again a narrower dispersion of the Er relaxation rates when lower Au fluences are implanted.

Cross-Section and Interaction Distance Estimation. A primary parameter that characterizes the energy-transfer process from Au_N nanoclusters to Er ions is the effective cross-section for Er sensitization, σ_{eff}. With the aim of providing an estimation of this parameter for the Er–Au coimplanted samples investigated in this work, we measured the Er^{3+} luminescent emission at 1540 nm as a function of the photon

dx.doi.org/10.1021/ph500452q | ACS Photonics 2015, 2, 96–104

flux with out-of-resonance excitation (at 476.5 nm). For the different sample series the measurements were performed on the samples annealed at the conditions that produce the highest PL emission at 1540 nm, i.e., characterized by the strongest sensitization effect ("best-performing" samples). For out-of-resonance pumping conditions the excitation of the Er ions occurs only indirectly, mediated by the energy transfer from the Au_N nanoclusters. From a phenomenological point of view, the process can be described by the following rate equation[16]

$$\frac{dN_{Er}^{*s}}{dt} = W_s - \frac{N_{Er}^{*s}}{\tau} \quad (1)$$

where N_{Er}^{*s} is the population of Er ions in the excited state sensitized by the Au_N nanoclusters and τ the Er emission lifetime in the Er−Au coimplanted samples. W_s represents the sensitization rate and describes the increase in the population of excited Er ions due to the energy transfer from the Au_N nanoclusters. W_s is proportional to the photon flux, ϕ, and can be written in the form $W_s = \sigma_{eff}\phi(f_s N_{Er}^{act} - N_{Er}^{*s})$, where σ_{eff} is the effective cross-section for Er ion excitation mediated by the Au_N sensitizers and f_s is the fraction of the total population of optically active Er ions (N_{Er}^{act}) that can be indirectly sensitized by the Au_N nanoclusters. By taking the steady-state solution of eq 1 and considering that the Er luminescent intensity is proportional to the excited Er population (i.e., $I_{PL} \propto N_{Er}^{*s}/\tau_{rad}$ where τ_{rad} is the radiative decay time of the Er excited state in the Er−Au coimplanted samples) the Er PL intensity will be given by the relation

$$I_{PL}(\phi) = K\left(f_s N_{Er}^{act}\frac{\tau}{\tau_{rad}}\frac{\sigma_{eff}\phi}{1+\sigma_{eff}\tau\phi}\right) = K\left(f_s N_{Er}^{act} Q\frac{\sigma_{eff}\phi}{1+\sigma_{eff}\tau\phi}\right) \quad (2)$$

$Q = \tau/\tau_{rad}$ is the quantum yield of the Er emission transition at 1540 nm in the Er−Au coimplanted samples; the constant K accounts for the collection efficiency of the PL setup. The effective cross-section σ_{eff} for Er sensitization can be estimated by fitting the experimental data with eq 2. As an example in Figure 4 we reported the PL intensity as a function of the photon flux of the samples Er1Au1−N720, Er1Au5−N620, and Er1Au10−N600. The solid lines are the best-fit results according to eq 2. The effective cross-sections estimated for all the "best-performing" samples are reported in Table 2. The numerical results have been calculated by using the effective Er emission lifetimes reported in Figure 3 ($\tau = \tau_{eff}$). The data are plotted in Figure 5 versus the [Au]/[Er] concentration ratio. The same symbols as in Figure 2 have been used to indicate the different Er content in the samples. The dashed line has to be used as a guide for the eye. The data in Figure 5 show that the trend of σ_{eff} as a function of the [Au]/[Er] concentration ratio is not monotonic: a maximum (of the order of 8×10^{-18} cm^2) is obtained for a concentration ratio [Au]/[Er] of about 5. It is important to compare the estimated sensitization cross-sections with the intrinsic emission cross-section of the Er^{3+} ions for the $^4I_{13/2} \rightarrow {}^4I_{15/2}$ transition (σ). To do this an independent determination of σ is necessary, and it can be obtained in principle by studying the PL emission properties of the Er800 reference sample for resonant excitation. Nonetheless, due to the low Er concentration in the samples (below 1% at.) and the reduced thickness of the Er containing layer (about 70 nm) a direct measurement of σ is difficult. In particular, the same approach used to determine σ_{eff} in the Er−Au coimplanted samples is not applicable in this case: no saturation effect or deviation from the linear trend was observed in the measurements of the PL emission intensity as a function of the photon flux of the Er800 reference sample up to the highest flux values achievable with the experimental setup, as shown in Figure 6. Instead, an indirect estimation of σ could be obtained by applying the Fuchtbauer−Ladenberg approach[33] to the analysis of the Er^{3+} emission spectrum. The inset in Figure 6 shows the room-temperature PL emission spectrum of the Er800 reference sample. By this approach we get $\sigma = 4.4 \times 10^{-21}$ cm^2 which is in good agreement with the cross-section values determined with different methods for various Er-implanted photonic materials.[6] Moreover the value of σ is more than 3 orders of magnitude lower than the effective cross-section for indirect Er ion excitation through energy transfer estimated for the Er−Au coimplanted samples (see Table 2), thus proving the remarkable effectiveness of Au molecular clusters as sensitizers for the Er emission.

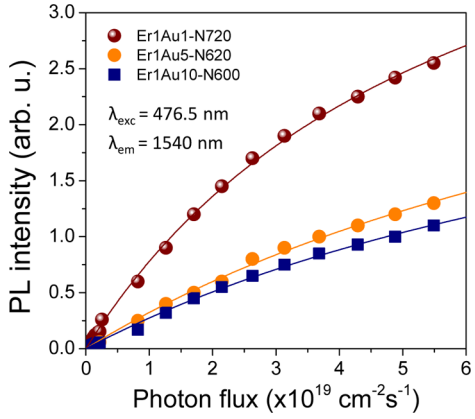

Figure 4. PL intensity measured at 1540 nm as a function of the photon flux of the samples indicated in the legend. The measurements have been performed with out-of-resonance excitation at 476.5 nm. The continuous lines are best fits to the data according to the model described in the text.

In order to quantitatively determine all the other photophysical parameters, such as the sensitized Er fractions, f_s, the quantum yields, Q, and particularly the interaction length between the Er ions and the Au_N nanoclusters, R_{int}, we investigated the Er^{3+} PL emission at 1540 nm versus photon flux with resonant excitation conditions. For resonant pumping (at 488 nm), the excitation of the Er ions may occur through two paths: indirectly, mediated by the energy transfer from the Au_N sensitizers, and directly by the pumping beam through the $^4I_{15/2} \rightarrow {}^4F_{7/2}$ Er absorption transition. To account for these two mechanisms, the PL emission intensity at 1540 nm measured by excitation at 488 nm can be written as a function of the photon flux as

$$I'_{PL}(\phi) = K\left(f'_s N_{Er}^{act} Q\frac{\sigma'_{eff}\phi}{1+\sigma'_{eff}\tau\phi} + f_d N_{Er}^{act} Q\sigma\phi\right) \quad (3)$$

The first term in the right-hand side of eq 3 describes the contribution to the PL signal arising from the fraction f'_s of the optically active Er ions indirectly sensitized by the Au_N nanoclusters, while the second term is introduced to take into account the direct excitation of the remaining fraction f_d ($f'_s + f_d = 1$). In this case the sensitized fraction is indicated as f'_s to

dx.doi.org/10.1021/ph500452q | ACS Photonics 2015, 2, 96−104

Table 2. Fitting Results According to the Model Described in the Text of the Er−Au Coimplanted Samples Annealed at the Conditions Corresponding to the Highest PL Emission at 1540 nm[a]

samples	[Au] × 10^{20} (at/cm^3)	R_c (nm)	σ_{eff} × 10^{-18} (cm^2)	f_s(out) (%)	f'_s(in) (%)	$\tilde{Q}$ (%)	R_{int}(out) (nm)	R'_{int}(in) (nm)
Er1Au0.5−N700	0.43 ± 0.04	0.31 ± 0.02	3.4 ± 0.8	0.49 ± 0.16	0.39 ± 0.08	26 ± 1	0.65 ± 0.07	0.61 ± 0.05
Er1Au1−N720	1.0 ± 0.1	0.34 ± 0.02	3.6 ± 0.2	1.00 ± 0.15	0.74 ± 0.10	73 ± 8	0.69 ± 0.05	0.63 ± 0.05
Er0.7Au1−N720	1.0 ± 0.1	0.34 ± 0.02	2.7 ± 0.2	1.64 ± 0.31	1.27 ± 0.22	34 ± 5	0.80 ± 0.07	0.74 ± 0.06
Er0.4Au1−N650	1.0 ± 0.1	0.31 ± 0.02	5.4 ± 0.9	0.61 ± 0.21	0.58 ± 0.15	49 ± 8	0.58 ± 0.07	0.57 ± 0.05
Er1Au5−N620	4.3 ± 0.4	0.38 ± 0.04	7.1 ± 0.8	0.29 ± 0.05	0.16 ± 0.02	50 ± 2	0.43 ± 0.04	0.41 ± 0.04
Er0.7Au5−N620	4.3 ± 0.4	0.38 ± 0.04	8.0 ± 1.1	0.26 ± 0.05	0.16 ± 0.02	44 ± 2	0.42 ± 0.04	0.40 ± 0.04
Er1Au10−N600	9.6 ± 0.9	0.43 ± 0.04	3.9 ± 0.5	0.73 ± 0.16	0.51 ± 0.08	30 ± 3	0.50 ± 0.05	0.48 ± 0.03

[a] R_c is the average radius of Au clusters in the samples as estimated by EXAFS.[34]

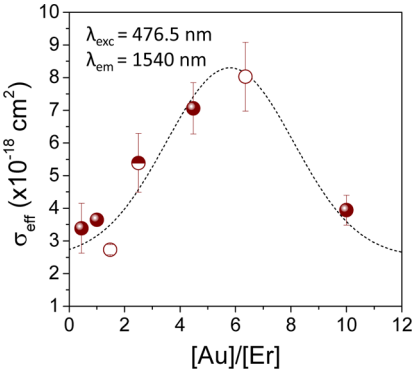

Figure 5. Effective cross-sections measured at 476.5 nm as a function of the [Au]/[Er] concentration ratio. The values have been estimated from the samples that exhibit the maximum PL emission of each sample series. The different symbols indicate the different Er content in the samples. The dashed line is reported as a guide for the eye.

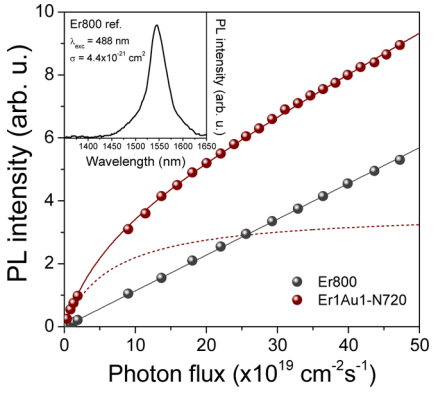

Figure 6. PL intensity measured at 1540 nm as a function of the photon flux of the samples Er1Au1−N720 (red dots) and the Er800 reference sample (gray dots). The measurements have been performed with resonant excitation at 488 nm. The continuous lines are best-fits to the data according to the model described in the text. The red dashed line represents the estimated contribution to the total PL signal of the sensitized Er fraction in the Er1Au1−N720 sample. Inset: Room temperature PL spectrum of the Er800 reference sample.

distinguish it from the corresponding value (f_s) in eq 2 since different sensitized fractions can be estimated for resonant and nonresonant Er excitation conditions. The explanation of this result will be discussed in detail further in the text. σ'_{eff} is the effective cross-section of the sensitization process for excitation at 488 nm. Since the energy transfer from the Au_N nanoclusters to the Er ions was demonstrated to be mediated by the broad-band interband absorption transitions at the Au_N nanoclusters,[25] σ'_{eff} can be related to the value estimated at 476.5 nm (σ_{eff}) through the relation $\sigma'_{eff} = (\alpha'/\alpha)\sigma_{eff}$ where α' and α are the absorption coefficients at 488 and 476.5 nm, respectively. For the samples investigated in this work a ratio $\alpha'/\alpha = 0.87$ was estimated by UV−vis absorption measurements. As an example, in Figure 6 we have reported the PL intensity measured at 1540 nm as a function of the photon flux of the sample Er1Au1−N720 (red dots) for excitation at 488 nm. The PL signal of the Er800 reference sample is also reported (gray dots). As mentioned above, in this case the PL emission increases linearly with the photon flux in the whole range explored, and it behaves according to the following expression

$$I^*_{PL}(\phi) = K(N_{Er}Q^*\sigma\phi) \tag{4}$$

where $Q^* = \tau^*/\tau^*_{rad}$ is the quantum yield of the Er800 reference sample. A reasonable estimation of $Q^* = 0.76$ can be obtained considering the measured decay time of the Er800 reference sample, $\tau^* = (10.7 \pm 0.1)$ ms, and using for τ^*_{rad} the value of 14.1 ms as given by Polman et al. in ref 6. Since the measurements of PL intensity versus photon flux of all the investigated samples have been collected with the same acquisition parameters as those used for the Er800 reference sample (i.e., the constant K in eqs 3 and 4 is the same), for the quantitative analysis we performed best fittings of the PL signal of the different Er−Au coimplanted samples normalized to that of the Er800 reference sample. This approach has the advantage of strongly improving the stability of the fitting algorithm providing more accurate results. Thus, the following expression can be written

$$\frac{I'_{PL}(\phi)}{I^*_{PL}(\phi)} = f'_s\xi\frac{\sigma'_{eff}}{\sigma}\frac{Q}{Q^*}\frac{1}{1+\sigma'_{eff}\tau\phi} + f_d\xi\frac{Q}{Q^*} \tag{5}$$

The parameter $\xi = N^{act}_{Er}/N_{Er}$ represents the fraction of optically active Er ions in the Er−Au coimplanted samples with respect to the population in the reference sample. This parameter accounts for all the possible effects that may reduce the population of optically active Er ions, thus giving $\xi \leq 1$. The main source of such an effect can be attributed to residual Au implantation damage not completely recovered after the annealing treatments. As mentioned above, we studied in the past the implantation damage effects on the Er^{3+} luminescence properties on Er−Xe coimplanted samples.[26] In that work Xe was implanted at two fluences (low and high) to reproduce the damage effects as in the Er1Au1 and Er1Au10 sample series. The results give $\xi \cong 1$ and $\xi \cong 0.4$ for the two fluences. Nonetheless, a direct determination of the parameter ξ in the samples investigated in the present work is not possible. For this reason the data have been fitted considering as free parameters only f'_s ($f'_s + f_d = 1$) and the term $\tilde{Q} = \xi Q$. A

dx.doi.org/10.1021/ph500452q | ACS Photonics 2015, 2, 96−104

summary of the obtained results for all the investigated samples is reported in Table 2. The red solid line in Figure 6 is the best-fit to the data of the sample Er1Au1−N720. The red dashed line is plotted for comparison to show the contribution to the total PL signal arising only from the fraction of Er ions indirectly sensitized through energy transfer by the Au_N nanoclusters, i.e., the first term in eq 3.

For all the investigated samples the estimated sensitized fractions are very small, below 1%. This means that in spite of the very high sensitization cross-sections demonstrated (see Figure 5) the number of Er ions that can be indirectly excited through the energy transfer from the Au_N nanoclusters is indeed much limited. Moreover, in all cases the sensitized fractions estimated for out-of-resonance pumping conditions result in systematically higher values than those obtained at resonant excitation ($f_s > f_s'$). A physical explanation of this result can be obtained by taking into account the interaction distance between Er ions and Au_N nanoclusters in the samples. In the hypothesis of a random distribution of Er ions and Au clusters, a quantitative estimation of the interaction volume V_{int} (i.e., the volume containing the fraction f_s of Er ions excited through the energy transfer from the Au_N sensitizers) can be obtained according to the relation

$$V_{int} = \frac{f_s N}{[Au]} = \frac{4\pi}{3}(R_{int}^3 - R_c^3) \quad (6)$$

where [Au] is the gold concentration in the samples and N is the average number of Au atoms per cluster. An estimation of N in the investigated samples was obtained by EXAFS analyses.[34] The ratio $[Au]/N$ thus represents the Au cluster concentration in the samples. The second equality in eq 6 can be used to determine the effective interaction radius R_{int} between the Au nanoclusters and the Er ions assuming the interaction volume as a spherical shell around the Au nanocluster. R_{int} thus represents the maximum distance from the center of the Au nanoclusters at which an Er ion can be sensitized with non-negligible efficiency. The average Au cluster radius, R_c, was calculated according to the relation: $R_c = R_a(N)^{1/3}$ (R_a = 0.1505 nm is the average radius of a Au atom in the cluster);[25] the values are reported in Table 2. The interaction radii determined with this method from the different samples investigated in the present work are reported in the last two columns in Table 2. For all the samples the results are in the range 0.4−0.8 nm. This demonstrates that the energy-transfer process from the Au_N nanoclusters to the Er^{3+} ions is indeed a short-range coupling mechanism occurring at interatomic distances. Furthermore, shorter interaction radii were systematically determined for excitation at 488 nm (R_{int}') with respect to the values estimated at 476.5 nm (R_{int}). Numerically, this is due to the fact that the sensitized fractions estimated from the analysis of PL data measured at 488 nm are systematically smaller than those evaluated at 476.5 nm for all the investigated samples. From the physical point of view, a tentative explanation of this result is sketched in Figure 7. For out-of-resonance pumping conditions (at 476.5 nm) the Er ions are excited only indirectly through the energy transfer from the Au_N nanoclusters. The efficiency of this process (ϵ_s) is very high due to the large effective cross-section for indirect sensitization, but it is expected to decrease monotonically by increasing the radial distance between the Au nanoclusters' surface and the Er ions (e.g., a typical r^{-6} dependence can be considered for dipolar coupling (Förster interaction), while an

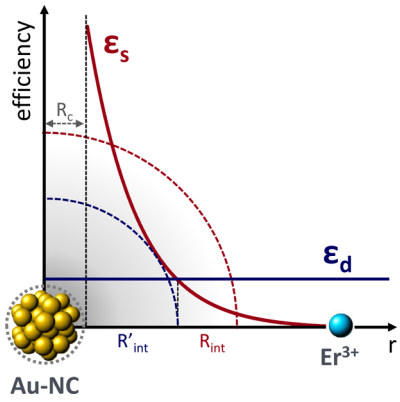

Figure 7. Schematic representation of the sensitization efficiency (ϵ_s) as a function of the radial distance r between the Au nanocluster and the Er^{3+} ion. ϵ_d is the efficiency for direct excitation of the Er^{3+} ions through absorption of the 488 nm pumping beam. R_{int}' and R_{int} are interaction distances estimated for in-resonance (at 488 nm) and out-of-resonance (at 476.5 nm) excitation conditions. Distances are not in scale.

exponential decay would be expected for exchange mechanims (Dexter interaction)[35−38]). Within this framework the estimated sensitization cross-sections have to be interpreted as a mean value over the interaction distance. Conversely, for resonant pumping conditions (at 488 nm) the excitation of the Er ions occurs both directly through the absorption of the incoming photons by the Er ions and indirectly, mediated by the energy transfer from the Au_N sensitizers. The efficiency of direct excitation (ϵ_d) is much lower than ϵ_s ($\sigma \ll \sigma_{eff}$) but can be considered constant across the sample. Therefore, at distances from the Au nanocluster's surface at which the efficiency for indirect sensitization of the Er ions becomes smaller than the one for direct excitation ($\epsilon_s(r) < \epsilon_d$), the direct excitation mechanism prevails. The interaction radius determined from the analysis of PL measurements performed at 488 nm (R_{int}') can be interpreted in this framework as an estimation of such a crossing point. At nonresonant pumping conditions, on the other hand, due to the lack of other competitive mechanisms also the Er ions lying at distances from the Au nanoclusters' surface corresponding to the tails of the efficiency curve contribute to the PL signal, giving rise to larger sensitized fractions and interaction radii.

A final comment is worth noting about a possible strategy to gain further enhancements of the Er emission efficiency. This is of paramount technological importance for the use of these systems in specific photonic devices. The idea is to exploit the nonresonant nature of the energy-transfer process that is mediated by the broad-band interband absorption of the Au nanoclusters. As an example, in Figure 8 we have reported the PL intensity as a function of the annealing temperature of the Er1Au1 samples, obtained with different pumping conditions: resonant excitation (at 488 nm), out-of-resonance condition (at 476.5 nm), and multiline pumping. In the last case all the emission lines of the Ar laser have been used at the same time to mimic a possible continuous broad-band pumping scheme. To quantitatively compare the intensities, due to the different power of the laser at the different emission wavelengths, the PL signals have been normalized to the laser power at 488 nm. The same behavior is observed for all the sample series: a slightly higher PL emission at 1540 nm is detected at all the annealing temperatures for out-of-resonance pumping conditions with

dx.doi.org/10.1021/ph500452q | ACS Photonics 2015, 2, 96−104

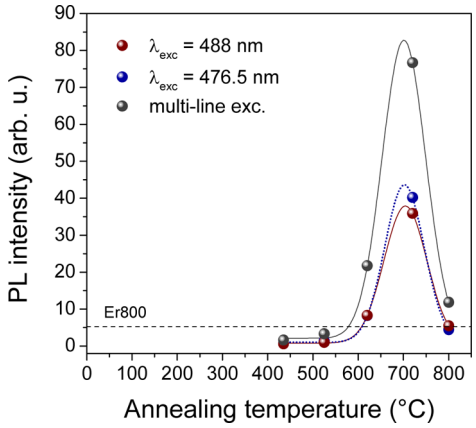

Figure 8. PL emission at 1540 nm as a function of the annealing temperature of samples Er1Au1 for the three different pumping conditions: in resonance (488 nm), out-of-resonance (476.5 nm), and multiline excitation. The intensities have been normalized to the laser power at 488 nm.

respect to resonant excitation, due to the slightly higher absorption cross-section of the Au clusters at λ = 476.5 nm with respect to λ = 488 nm. Such an effect is strongly amplified when the multiline pumping is used, with an increase of more than a factor of 2 in the PL peak intensity, that results in this case in an amplification of the Er emission signal of 17 times with respect to the reference sample.

CONCLUSIONS

The effect of Au_N molecular clusters as sensitizing agents of the Er^{3+} luminescence in Er–Au coimplanted silica has been elucidated. In particular, the investigation of systems in which the [Au]/[Er] concentration ratio was spanned over more than 1 order of magnitude allowed us to develop a simple phenomenological model for the Er sensitization mediated by energy transfer from Au_N nanoclusters through which the most important photophysical parameters, such as the sensitized fractions, the effective cross-section, and the interaction distance of the energy-transfer process, have been determined. This result is particularly important since, up to now, a detailed knowledge of these parameters was lacking, whereas on the contrary they take on a key role both to unveil the physical mechanisms that trigger the energy transfer between gold molecular clusters and Er ions and, from a more applicative point of view, to effectively exploit these processes in advanced photonic devices. The results revealed that the sensitization mechanism is characterized by a large effective cross-section, more than 3 orders of magnitude larger than the intrinsic cross-section for Er emission. Moreover, we found that the energy-transfer is a short-range coupling occurring at interatomic distances in the range 0.4–0.8 nm. Nonetheless, in spite of the very large cross-section of the process, it was also demonstrated that only a limited fraction of the Er ions can be indirectly excited by energy transfer from the Au_N nanoclusters and that better performances can be achieved by increasing the Er concentration (of course, without exceeding the concentration quenching threshold). Finally, a further boost of the PL emission performances can be gained by broad-band pumping and thus exploiting the nonresonant nature of the energy-transfer process demonstrated between the Au_N molecular clusters and the Er ions.

ASSOCIATED CONTENT

Supporting Information

Additional experimental details. This material is available free of charge via the Internet at http://pubs.acs.org/.

AUTHOR INFORMATION

Corresponding Author

*E-mail: tiziana.cesca@unipd.it.

Notes

The authors declare no competing financial interest.

ACKNOWLEDGMENTS

This work has been partially supported by the Progetto di Ateneo CPDA 101587 of the University of Padova, Italy.

REFERENCES

(1) Binnemans, K. Lanthanide-Based Luminescent Hybrid Materials. *Chem. Rev.* **2009**, *109*, 4283–4374.
(2) Hüffner, S.. *Optical Spectra of Transparent Rare-Earth Compounds*; Academic Press, New York, 1978.
(3) Ende, B. M. v. d.; Aarts, L.; Meijerink, A. Lanthanide ions as spectral converters for solar cells. *Phys. Chem. Chem. Phys.* **2009**, *11*, 11081–11095.
(4) Luo, W.; Fu, C.; Li, R.; Liu, Y.; Zhu, H.; Chen, X. Er^{3+}-Doped Anatase TiO_2 Nanocrystals: Crystal-Field Levels, Excited-State Dynamics, Upconversion, and Defect Luminescence. *Small* **2011**, *7*, 3046–3056.
(5) Miniscalco, W. J. Erbium-doped glasses for fiber amplifiers at 1500 nm. *J. Lightwave Technol.* **1991**, *9*, 234–250.
(6) Polman, A. Erbium implanted thin film photonic materials. *J. Appl. Phys.* **1997**, *82*, 1–39.
(7) Kenyon, A. J. Erbium in silicon. *Semicond. Sci. Technol.* **2005**, *20*, R65–R84.
(8) Kenyon, A. Recent developments in rare-earth doped materials for optoelectronics. *Prog. Quant. Electron.* **2002**, *26*, 225–284.
(9) Molard, Y.; Labbé, C.; Cardin, J.; Cordier, S. Sensitization of Er^{3+} Infrared Photoluminescence Embedded in a Hybrid Organic-Inorganic Copolymer containing Octahedral Molybdenum Clusters. *Adv. Funct. Mater.* **2013**, *23*, 4821–4825.
(10) Yin, C.; Rancic, M.; de Boo, G. G.; Stavrias, N.; McCallum, J. C.; Sellars, M. J.; Rogge, S. Optical addressing of an individual erbium ion in silicon. *Nature* **2013**, *497*, 91–94.
(11) Bertaina, S.; Gambarelli, S.; Tkachuk, A.; Kurkin, I. N.; Malkin, B.; Stepanov, A.; Barbara, B. Rare-earth solid-state qubits. *Nat. Nanotechnol.* **2007**, *2*, 39–42.
(12) Hehlen, M. P.; Cockroft, N. J.; Gosnell, T. R.; Bruce, A. J. Spectroscopic properties of Er^{3+}- and Yb^{3+}-doped soda-lime silicate and aluminosilicate glasses. *Phys. Rev. B* **1997**, *56*, 9302–9318.
(13) Strohhofer, C.; Polman, A. Absorption and emission spectroscopy in Er^{3+}-Yb^{3+}-doped aluminum oxide waveguides. *Opt. Mater.* **2003**, *21*, 705–712.
(14) Fuji, M.; Yoshida, M.; Kanzawa, Y.; Hayashi, S.; Yamamoto, K. 1.54 μm photoluminescence of Er^{3+} doped into SiO_2 films containing Si nanocrystals: evidence for energy transfer from Si nanocrystals to Er^{3+}. *Appl. Phys. Lett.* **1997**, *71*, 1198–1200.
(15) Chryssou, C. E.; Kenyon, A. J.; Iwayama, T. S.; Pitt, C. W.; Hole, D. E. Evidence of energy coupling between Si nanocrystals and Er^{3+} in ion-implanted silica thin films. *Appl. Phys. Lett.* **1999**, *75*, 2011–2013.
(16) Franzò, G.; Vinciguerra, V.; Priolo, F. The excitation mechanism of rare-earth ions in silicon nanocrystals. *Appl. Phys. A: Mater. Sci. Process.* **1999**, *69*, 3–12.
(17) Kik, P. G.; Brongersma, M. L.; Polman, A. Strong exciton-erbium coupling in Si nanocrystal-doped SiO_2. *Appl. Phys. Lett.* **2000**, *76*, 2325–2327.

(18) Pacifici, D.; Franzò, G.; Priolo, F.; Iacona, F.; Dal Negro, L. Modeling and perspectives of the Si nanocrystals-Er interaction for optical amplification. *Phys. Rev. B* **2003**, *67*, 245301-1−13.
(19) Enrichi, F.; Mattei, G.; Sada, C.; Trave, E.; Pacifici, D.; Franzò, G.; Priolo, F.; Iacona, F.; Prassas, M.; Falconieri, M.; Borsella, E. Study of the energy transfer mechanism in different glasses co-doped with Si nanoaggregates and Er^{3+} ions. *Opt. Mater.* **2005**, *27*, 904−909.
(20) Strohhofer, C.; Polman, A. Silver as a sensitizer for erbium. *Appl. Phys. Lett.* **2002**, *81*, 1414−1416.
(21) Martucci, A.; et al. Silver sensitized erbium doped ion exchanged sol gel waveguides. *Appl. Phys. A: Mater. Sci. Process.* **2004**, *80*, 557−563.
(22) Portales, H.; Mattarelli, M.; Montagna, M.; Chiasera, A.; Ferrari, M.; Martucci, A.; Mazzoldi, P.; Pelli, S.; Righini, G. Investigation of the role of silver on spectroscopic features of Er^{3+}-activated Ag-exchanged silicate and phosphate glasses. *J. Non-Cryst. Solids* **2005**, *351*, 1738−1742.
(23) Trave, E.; Mattei, G.; Mazzoldi, P.; Pellegrini, G.; Scian, C. Sub-nanometric metallic Au clusters as efficient Er^{3+} sensitizers in silica. *Appl. Phys. Lett.* **2006**, *89*, 151121-1−3.
(24) Mattarelli, M.; Montagna, M.; Vishnubhatla, K.; Chiasera, A.; Ferrari, M.; Righini, G. C. Mechanisms of Ag to Er energy transfer in silicate glasses: a photoluminescence study. *Phys. Rev. B* **2007**, *75*, 1−125102−6.
(25) Maurizio, C.; Trave, E.; Perotto, G.; Bello, V.; Pasqualini, D.; Mazzoldi, P.; Battaglin, G.; Cesca, T.; Scian, C.; Mattei, G. Enhancement of the Er^{3+} luminescence in Er-doped silica by few-atom metal aggregates. *Phys. Rev. B* **2011**, *83*, 195430-1−11.
(26) Cesca, T.; Maurizio, C.; Kalinic, B.; Perotto, G.; Mazzoldi, P.; Trave, E.; Battaglin, G.; Mattei, G. Implantation damage effects on the Er^{3+} luminescence in silica. *Opt. Express* **2012**, *20*, 16639−16649.
(27) Eichelbaum, M.; Rademann, K. Plasmonic Enhancement or Energy Transfer? On the Luminescence of Gold-, Silver-, and Lanthanide-Doped Silicate Glasses and Its Potential for Light-Emitting Devices. *Adv. Funct. Mater.* **2009**, *19*, 2045−2052.
(28) Cesca, T.; Kalinic, B.; Maurizio, C.; Scian, C.; Battaglin, G.; Mazzoldi, P.; Mattei, G. Near-infrared room temperature luminescence of few-atom Au aggregates in silica: a path for the energy-transfer to Er^{3+} ions. *Nanoscale* **2013**, *6*, 1716−1724.
(29) Cesca, T.; Kalinic, B.; Michieli, N.; Maurizio, C.; Scian, C.; Devaraju, G.; Battaglin, G.; Mazzoldi, P.; Mattei, G. Energy-transfer from ultra-small Au nanoclusters to Er^{3+} ions: a short-range mechanism. *Phys. Chem. Chem. Phys.* **2014**, DOI: 10.1039/C4CP01680G.
(30) Khosrofian, J. M.; Garetz, B. A. Measurement of a Gaussian laser beam diameter through the direct inversion of knife-edge data. *Appl. Opt.* **1983**, *22*, 3406−3410.
(31) Priolo, F.; Franz, G.; Pacifici, D.; Vinciguerra, V.; Iacona, F.; Irrera, A. Role of the energy transfer in the optical properties of undoped and Er-doped interacting Si nanocrystals. *J. Appl. Phys.* **2001**, *89*, 264−272.
(32) Bao, J.; Yu, N.; Capasso, F.; Mates, T.; Troccoli, M.; Belyanin, A. Controlled modification of erbium lifetime in silicon dioxide with metallic overlayers. *Appl. Phys. Lett.* **2007**, *91*, 131103-1−3.
(33) Barnes, W.; Laming, R.; Tarbox, E.; Morkel, P. Absorption and emission cross section of Er^{3+} doped silica fibers. *IEEE J. Quantum Electron.* **1991**, *27*, 1004−1010.
(34) Maurizio, C.; Cesca, T.; Perotto, G.; Kalinic, B.; Michieli, N.; Scian, C.; Joly, Y.; Battaglin, G.; Mazzoldi, P.; Mattei, G. 2014, submitted.
(35) Lakowicz, J.*Principles of Fluorescence Spectroscopy*; Springer, New York, 2006.
(36) Förster, T. Zwischenmolekulare Energiewanderung und Fluoreszenz. *Annal. Phys.* **1948**, *437*, 55−75.
(37) Dexter, D. L. A. Theory of Sensitized Luminescence in Solids. *J. Chem. Phys.* **1953**, *21*, 836−850.
(38) Julsgaard, B.; Lu, Y.-W.; Skougaard Jensen, R. V.; Pedersen, T. G.; Pedersen, K.; Chevallier, J.; Balling, P.; Nylandsted Larsen, A. Er sensitization by a thin Si layer: Interaction-distance dependence. *Phys. Rev. B* **2011**, *84*, 085403-1−7.